Injection Molding of Semicrystalline Polymers. I. Material Characterization

A. I. ISAYEV,* T. W. CHAN, K. SHIMOJO, and M. GMEREK

Institute of Polymer Engineering, University of Akron, Akron, Ohio 44325-0301

SYNOPSIS

Various material data for an isotactic polypropylene were acquired for the simulation of the injection molding of this material. Viscosity as a function of shear rate and temperature was measured using a capillary rheometer at high shear rates and a cone-and-plate rheometer at low shear rates. Heat-flow properties, characterizing kinetics and induction time of quiescent crystallization, were obtained from DSC measurements. Material data characterizing shear-induced crystallization were obtained from extrusion experiments through a slit die with subsequent quenching of the material in the die after various rest times. The thickness of the shear-induced crystallization layer was measured along with the birefringence in this layer. A model of shear-induced crystallization developed by Janeschitz-Kriegl and co-workers was used to fit the kinetic data. Thus, kinetic parameters such as the limiting shear rate below which no shear-induced crystallization can occur and the characteristic time for the relaxation of birefringence were obtained. © 1995 John Wiley & Sons, Inc.

INTRODUCTION

In injection molding, there exists a distribution of shear and normal stresses in the molten polymer form the wall to the center of the mold. It is well known from experimental experience that for semicrystalline polymers the high shear stresses near the wall give rise to an oriented lamella structure called the shear-induced crystallization or skin layer of the part. This skin layer is characterized by high birefringence and is responsible for such undesirable features as cleavability, warping, and stress whitening.[1] The polymer in the core region that does not incur high stresses is allowed to crystallize three-dimensionally to form spherulites. This distinct skin–core morphology is visible under a polarizing optical microscope. A third intermediate layer is usually seen as well, whereas other techniques such as X-ray diffraction have revealed up to five layers in some instances.[2–15] A review on the microstructure of injection-molded semicrystalline polymers was given by Katti and Schultz.[16]

Studies on shear-induced crystallization kinetics of polymers have been outnumbered considerably by those on quiescent (or thermally induced) crystallization kinetics. The first attempt to investigate both theoretically and experimentally the crystallization kinetics of a molten polymer subjected to a constant shear stress appears to be by Kobayashi and Nagasawa.[17] A recent and comprehensive review on the subject was given by Eder et al.[1] Quite a few experimental elucidations of the mechanism of shear-induced crystallization have appeared over the years,[1,18–34] though most of them only offer qualitative understanding. Not until the works of Janeschitz-Kriegl and co-workers[1,32,35,36] does a theory of shear-induced crystallization become available that offers the possibility for kinetic parameters to be determined from independent experiments and, as such, is applicable to the simulation of injection molding. Before that, the modeling of crystallization in injection molding had to rely on kinetic models that either did not consider the effects of shear[37–44] or took into account the effects of shear in a purely empirical manner such that the model parameters

This article is dedicated to Professor Hermann Janeschitz-Kriegl on the occasion of his 70th birthday.

* To whom correspondence should be addressed.

Journal of Applied Polymer Science, Vol. 55, 807–819 (1995)
 CCC 0021-8995/95/050807-13

were not readily susceptible to experimental determinations.[45,46]

This is Part I of a study on the injection molding of crystallizable polymers. The purpose here was to acquire various data for the simulation of the injection molding of a polypropylene (PP) to be carried out in Part II.[47] The modified Cross model[48] was fitted to the viscosity data obtained from a capillary rheometer at high shear rates and a cone-and-plate rheometer at low shear rates. Heat-flow properties, characterizing the kinetics and induction time of quiescent crystallization, were taken from nonisothermal DSC measurements. The theory of Janeschitz-Kriegl et al.[1,35,36] was used to describe shear-induced crystallization kinetics. Shear-induced crystallization properties such as the limiting shear rate below which no shear-induced crystallization occurs and the relaxation time for shear-induced crystallization were determined from extrusion experiments using a special slit die apparatus. In Part II,[47] the same model parameters obtained here in Part I will be used to simulate the injection-molding process. Experimental results from injection-molding experiments will be presented and compared with simulated results.

THEORY OF QUIESCENT CRYSTALLIZATION

For the kinetic description of quiescent crystallization occurring in the core region of the molding, we use the differential form of the Nakamura equation:[49,50]

$$\frac{d\xi}{dt} = nK(T)(1 - \xi)[-\ln(1 - \xi)]^{(n-1)/n} \quad (1)$$

where ξ is the degree of crystallinity; K, the rate constant; n, the Avrami index; T, the temperature, and t, the time. The Nakamura equation was developed on the basis of isokinetic conditions and the assumption that the number of activated nuclei is a constant.[49,50] Thus, the temperature dependence of the rate constant K may be given by the Hoffman–Lauritzen expression:[50,51]

$$K(T) = (\ln 2)^{1/n}\left(\frac{1}{t_{1/2}}\right)_0 \exp\left(-\frac{U^*/R}{T - T_\infty}\right) \times \exp\left(-\frac{K_g}{T\Delta T f}\right) \quad (2)$$

where $\Delta T = T_m^0 - T$ and $f = [(2T)/(T + T_m^0)]$. In the Hoffman–Lauritzen expression, R is the universal gas constant; T_m^0, the equilibrium melting point; and f, a correction factor for the reduction in the latent heat of fusion as the result of a decrease in temperature. Thus expressed, the kinetic model has four parameters in addition to n: $(1/t_{1/2})_0$ is a preexponential factor that includes all terms independent of temperature; U^*, the activation energy for segmental jump rate and may be given a universal value of 6284 J/mol, K_g is the nucleation exponent, and T_∞ may be taken as the glass-transition temperature minus 30K.

The Nakamura equation does not make allowance for an induction period for nucleation. To determine the induction time for quiescent crystallization, the method of Sifleet et al.[52] is used. The nonisothermal induction time can be obtained by a summation of isothermal induction times according to

$$\int_0^{t_I} \frac{dt}{t_i(T)} = 1 \quad (3)$$

where t_i is the isothermal induction time, and t_I, the nonisothermal induction time. For melt-crystallization, the isothermal induction time is assumed to follow the Godovsky and Slonimsky[53] expression:

$$t_i = t_m(T_m^0 - T)^{-a} \quad (4)$$

where t_m and a are material constants independent of temperature.

THEORY OF SHEAR-INDUCED CRYSTALLIZATION

A theory of shear-induced crystallization has been developed by Janeschitz-Kriegl and co-workers.[1,35,36] This theory assumes that the locations of nucleation are created by the flow. Also, these precursors of nucleation can disappear by a relaxation process after the flow is stopped. However, if the sheared melt is quenched quickly enough, shear-induced crystallization will occur. This type of crystallization is characterized by lamellar crystals oriented in one dimension.

According to this theory, the probability θ for a precursor to form is given by a first-order differential equation:

$$\frac{d\theta}{dt} = \left(\frac{\dot\gamma}{\dot\gamma_a}\right)^2 \frac{1 - \theta}{\tau} - \frac{\theta}{\tau} \quad (5)$$

where $\dot\gamma$ is the shear rate; $\dot\gamma_a$, the critical shear rate of activation; and τ, the relaxation time for shear-

induced crystallization. The first term on the right-hand side of eq. (5) is the creation term. Once θ reaches the value of unity, no further improvement of the aptitude for shear-induced crystallization can be achieved. The second term on the right-hand side describes the decay of θ. This is the simplest differential equation that can explain (at least qualitatively) shear-induced crystallization. The parameters $\dot{\gamma}_a$ and τ are strong functions of the melt temperature. Here, they are both assumed to have an Arrhenius-type temperature dependence given by

$$\dot{\gamma}_a = \dot{\gamma}_{a0}\exp\left(-\frac{E_a}{RT}\right) \tag{6}$$

and

$$\tau = \tau_0\exp\left(\frac{E_\tau}{RT}\right) \tag{7}$$

where $\dot{\gamma}_{a0}$, E_a, τ_0, and E_τ are material constants independent of temperature.

For a tentative description of shear-induced crystallization kinetics, Janeschitz-Kriegl and coworkers introduced the "model of uttermost uniformity."[1,36] This model assumes that the crystals grow in three dimensions, though not necessarily to the same extent, and the growth rates and the nucleation rate have the same temperature dependence. These are oversimplifying assumptions, of course. For one, the crystal growth in shear-induced crystallization should probably be closer to one-dimensional than to three-dimensional, as Eder et al.[54] would later acknowledge. As to the second, it is simply the isokinetic assumption made in the development of the widely used Nakamura equation for quiescent crystallization. With these assumptions, it can be shown[1] that

$$\frac{d\Psi_1}{dt} = \left(\frac{\dot{\gamma}}{\dot{\gamma}_a}\right)^2\frac{1-\Psi_1}{\tau} - \frac{\Psi_1}{\tau} \tag{8}$$

$$\Psi_1 = \frac{1}{\hat{g}}\left(\frac{d\Psi_0}{dt}\right) \tag{9}$$

$$\Psi_0 = \left[\frac{\Psi_0(t)}{2}\right]^{1/4} \tag{10}$$

and

$$\phi_0 = -\ln(1-\xi) \tag{11}$$

where $\Psi_1 \equiv \theta$; $\hat{g}$ is the geometric mean of the growth rates and the nucleation rate; ϕ_0, the unrestricted fraction of crystal volume; and ξ, the degree of crystallinity. It is noted that this approach to shear-induced crystallization is, in many respects, parallel to that taken by Schneider et al.[55,56] in developing a set of differential rate equations for quiescent crystallization.

Janeschitz-Kriegl and co-workers[1,26,27,29,36] observed that with high-temperature shearing where no crystallization occurred in a continuous flow the typical textures of shear-induced crystallization were obtained, nevertheless, when the sample was quenched immediately or with some delay after cessation of flow. Accordingly, the model parameters $\dot{\gamma}_a$, τ, and $\hat{g}$ may be determined from a special kind of extrusion experiments at temperatures well above the melting point, keeping the shearing time t_s shorter than the induction time for shear-induced crystallization of the melt. Once the flow is stopped at a time t_s, the sample is quenched to a temperature well below the melting point. For this case, it can be shown[1] that

$$\frac{t_s}{\tau} = \frac{-\ln\left[(1-A)\left(1-\frac{\dot{\gamma}_l^2}{\dot{\gamma}^2}\right)\right]}{1+\frac{\dot{\gamma}^2}{\dot{\gamma}_l^2}\frac{A}{(1-A)}} \tag{12}$$

and

$$\dot{\gamma}_a = \dot{\gamma}_l\left(\frac{1}{A}-1\right)^{1/2} \tag{13}$$

where parameter A is related to the ratio of the growth rates of quiescent crystallization and shear-induced crystallization, and $\dot{\gamma}_l$, the limiting shear rate below which no shear-induced crystallization can occur after quenching to a temperature below the melting point. Parameters A and $\dot{\gamma}_l$ at a given temperature can be obtained by fitting eq. (12) to the experimental data of the shearing time vs. the shear rate. Once A and $\dot{\gamma}_l$ are determined, the value of $\dot{\gamma}_a$ is calculated from eq. (13).

The parameter $\hat{g}$ is given by

$$\hat{g} = \frac{[-\ln(1-\varepsilon)/2]^{1/4}}{At_i(T)} \tag{14}$$

where $t_i(T)$ is the isothermal induction time for quiescent crystallization, and ε, the smallest measurable value of crystallinity that is observed when the induction time is reached. Here, ε is taken to be 0.01. In arriving at eq. (14), it is assumed that the induction time for the sheared melt after quenching

to a lower temperature is the same as that for a quiescent melt at the same temperature.[1]

Parameters $\dot{\gamma}_a$ and τ can only be determined for a narrow range of temperatures above the melting point where no crystallization occurs. The parameter $\hat{g}$, which is certainly also a strong function of temperature, is zero in this temperature range. The values of $\dot{\gamma}_a$ and τ at temperatures where $\hat{g}$ is significant have to be obtained by extrapolation using eqs. (6) and (7), respectively. In eq. (14), t_i is finite only at temperatures below the melting point, whereas the quantity A can be obtained experimentally only at temperatures above the melting point. Thus, either A or t_i has to be obtained by extrapolation for the purpose of determining $\hat{g}$. Fortunately, as will be shown below in Table II, parameter A tends to approach unity as the temperature drops below 185°C, at least for the PP studied here.

EXPERIMENTAL

Material

The material studied was a commercial-grade isotactic polypropylene (iPP) Pro-fax 6523 (Lot # BE37228) supplied by Himont USA, Inc. The melt flow index was 4.1 dg/min (230°C, 2.16 kg). The weight-average molecular weight and polydispersity index were 3.51×10^5 and 4.3, respectively.

Rheological Characterization

To determine the parameters in the modified Cross model,[48] viscosity measurements were performed on a Rheometrics mechanical spectrometer (RMS-800) in the cone-and-plate mode in the shear rate range 10^{-2} to 10^1 s^{-1} and on an Instron capillary rheometer (Model 3211) up to 10^3 s^{-1}. Measurements were made at three different temperatures: 180, 200, and 230°C.

Quiescent Crystallization Characterization

A Perkin-Elmer differential scanning calorimeter (DSC-7) was used to measure the nonisothermal crystallization kinetics. All measurements were carried out with the sample in a nitrogen atmosphere. Samples about 5 mg were weighed into standard aluminum pans and sealed. The samples were first heated to 200°C and kept for 10 min in the DSC furnace to erase any thermal history. The melted samples were then cooled at constant rates of 2.5, 5, 10, and 20°C/min. Before the PP samples were tested, pure indium was used to calibrate not just the temperature scale and the melting enthalpy, but also the heat-transfer coefficient between the sample pan and the DSC furnace.[57-59] All nonisothermal crystallinity results were corrected for the effects of temperature lag between the sample and the DSC furnace according to the method of Janeschitz-Kriegl et al.[57-59]

Shear-induced Crystallization Characterization

Isothermal shearing experiments were conducted on a single-screw extruder (Killion KL-100). A slit die apparatus was placed at the end of the extruder. The slit die apparatus is made of stainless steel. It consists of an inner cylinder that fits snugly when inserted into a cylindrical outer shell. A rectangular flow channel is cut in the central portion of the inner cylinder. The length, width, and height of the flow channel are 63.5, 16, and 1.6 mm, respectively. A single bolt holds the inner cylinder firmly in place during extrusion. The use of only one retaining bolt facilitates the removal of the inner cylinder from the outer shell after stoppage of flow. Experiments were carried out at four different temperatures: 185, 190, 200, and 210°C.

There are two controlling variables in these experiments: One was the flow rate and the other was the temperature. Heating was provided by three band heaters in the extruder and one on the die assembly. The screw rotation speed was adjusted before the flow was initiated. The material temperature was measured at the die exit using a thermocouple. The set points on the temperature controllers were adjusted until the temperature of the exiting melt reached the desired value. The flow rate was determined from the amount of extruded material within a given period of time. The flow was stopped after steady state had been reached. The inner part of the slit die assembly was then quenched rapidly in water at ambient temperature. Quenching was performed at various rest times after the cessation of flow. Once the sample was cooled, it was taken out of the die and cut according to Figure 1 using a diamond saw (Buehler Isomet Low Speed) and a microtome (Reichert Histo STAT Rotary). The final thickness of the sample was 20–25 μm. The thin sample was set on glass slides. The crystallization layers were observed under a polarizing optical microscope (Leitz Laborlux 12 POL) and the thickness of the skin layer was measured. The birefringence of the skin layer was determined from optical retardation measurements with the help of a compensator (Leitz tilting compensator). The optical retardation Γ was

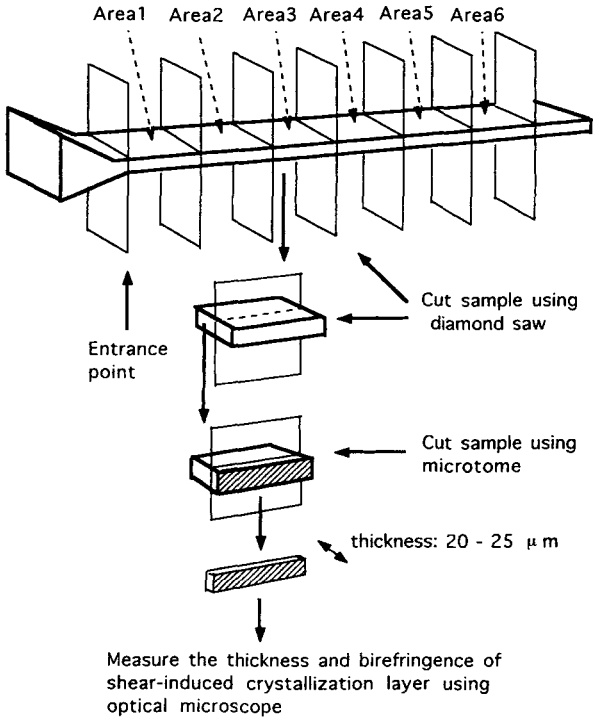

Figure 1 Sample cutting procedure in extrusion samples.

calculated using a Leitz calibration chart. The birefringence Δn is the optical retardation divided by the thickness of the sample.

RESULTS AND DISCUSSION

Rheological Data

Plots of steady shear viscosity vs. shear rate at three different temperatures for the PP used in this study are shown in Figure 2. The various symbols represent the experimental data and the solid lines represent the fitted values using the modified Cross model:[48]

$$\eta(\dot{\gamma}) = \frac{\eta_0(T)}{1 + \left(\frac{\eta_0(T)\dot{\gamma}}{\tau^*}\right)^{1-m}} \tag{15}$$

where

$$\eta_0(T) = B \exp\left(\frac{T_b}{T}\right) \tag{16}$$

The model parameter values B = 0.2 Pa-s, T_b = 5066.5 K, τ^* = 1.2 × 10^4 Pa, and m = 0.34 were found to fit the viscosity data well.

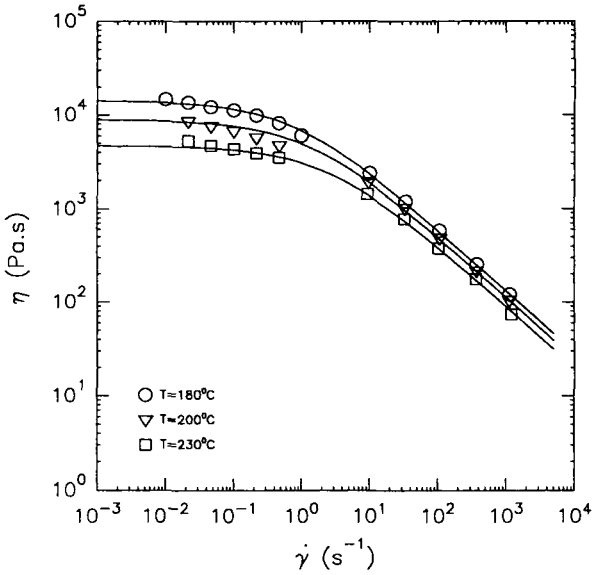

Figure 2 Viscosity as a function of shear rate at three different temperatures. Symbols and lines represent experimental and fitted values, respectively.

Quiescent Crystallization Constants

Heat-flow curves of DSC cooling runs at four different cooling rates are shown in Figure 3. It can be seen that the crystallization peaks for different cooling rates begin at different temperatures. With the increase of cooling rate, the starting point of the crystallization peak moves to a lower temperature. The nonisothermal induction time t_I was defined as

$$t_I = \frac{T_m^0 - T_c}{b} \tag{17}$$

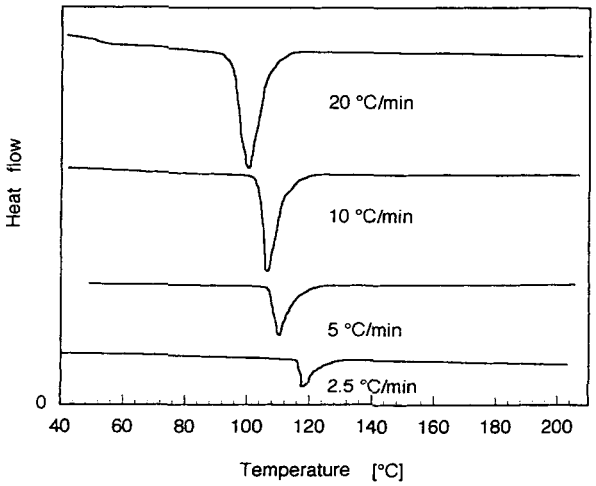

Figure 3 Heat-flow curves of DSC cooling runs at four different cooling rates.

Table I Temperature at Start of Crystallization and Nonisothermal Induction Time at Various Cooling Rates

Cooling Rate (°C/min)	Temperature at Start of Crystallization (°C)	Nonisothermal Induction Time (s)
2.5	128.3	1048.8
5.0	124.1	574.8
10.0	120.5	309.0
20.0	114.3	173.1

where T_m^0 is the equilibrium melting point (= 172°C for PP[60]); T_c, the temperature at which the crystallization peak begins; and b, is the cooling rate. The values of t_I and T_c for different cooling rates are given in Table I. By dividing the time into small intervals Δt and substituting eq. (4) in eq. (3),

$$\sum_0^{t_I} \frac{1}{t_m(T_m^0 - T)^{-a}} \Delta t = 1 \tag{18}$$

By fitting eq. (18) to the nonisothermal induction time data given in Table I using nonlinear regression, the following isothermal induction time parameters were obtained: $t_m = 8 \times 10^{11}$ s K^6 and $a = 6$. Figure 4 shows the fit of the induction time model [eq. (18)] to the experimental data. Using the same model parameters, the nonisothermal induction time for any thermal history can be calculated.

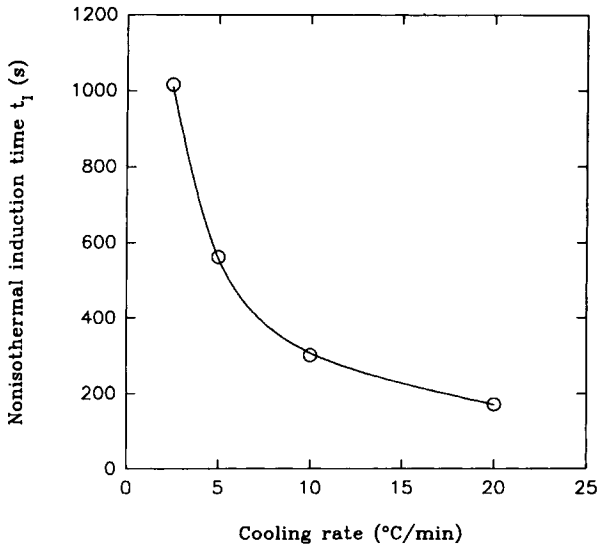

Figure 4 Nonisothermal induction time as a function of cooling rate. Symbols and lines represent experimental and fitted values, respectively.

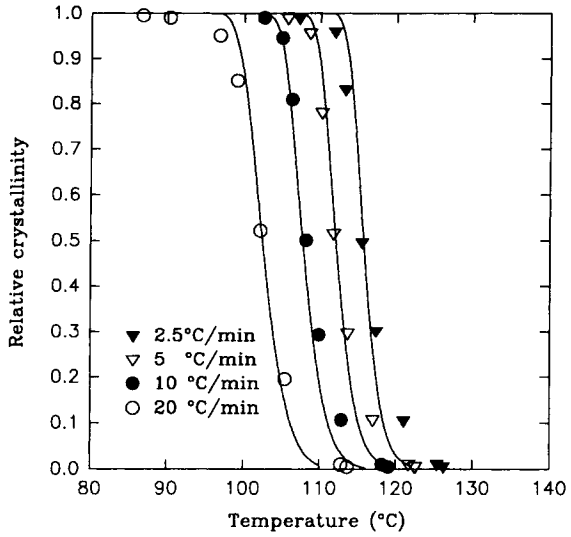

Figure 5 Relative crystallinity as a function of temperature at four different cooling rates. Symbols and lines represent experimental and fitted values, respectively.

Figure 5 shows the relative crystallinity as a function of temperature at four different cooling rates. These data were corrected for the effects of temperature lag between the sample and the DSC furnace according to the method of Janeschitz-Kriegl et al.[57-59] The relative crystallinity ξ was calculated according to

$$\xi = \frac{\Delta H_{T_c \to T}}{\Delta H_c} \tag{19}$$

where $\Delta_{T_c \to T}$ is the area under the heat-flow curve from T_c to T, and ΔH_c, the total area under the heat-flow curve. The crystallization kinetic model [eqs. (1) and (2)] was fitted to the data given in Figure 5 using nonlinear regression, assuming that the Avrami index $n = 3$. The following parameter values were obtained: $(1/t_{1/2})_0 = 2.07 \times 10^6$ s^{-1} and $K_g = 2.99 \times 10^5$ K^2. The fitted values are given by solid lines in Figure 5.

Shear-induced Crystallization Parameters

Shear-induced crystallization experiments were performed at several temperatures for two purposes: One purpose was to observe the growth of the skin layer using a polarized optical microscope. From this, the critical shear rate of activation $\dot{\gamma}_a$ for shear-induced crystallization can be obtained as a function of temperature. The other purpose was to study the relaxation behavior of the skin layer by the tech-

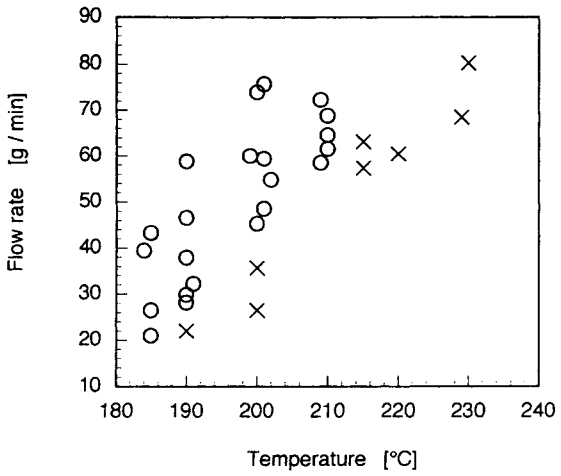

Figure 6 Experimental conditions for existence of shear-induced crystallization layer.

nique of birefringence. From this, the characteristic time τ for the relaxation of shear-induced crystallization can be determined as a function of temperature.

Development of Shear-induced Crystallization Layer

The rest time was negligible in this type of experiment, i.e., the inner part of the slit die assembly was dropped into the water bath as quickly as possible after the flow was stopped. Figure 6 shows the various conditions of flow rate and temperature for the existence of a skin layer. In this figure, the symbol "O" means that there exists a skin layer at 15 mm from the die entrance under the conditions indicated and the symbol "×" means no skin layer. It can be seen that as the temperature increases the minimum flow rate at which the skin layer appears increases.

The maximum screw rotation speed allowed in the Killion extruder was 95 rpm. This translates into a maximum flow rate of about 80 g/min for our PP in the temperature range 185–210°C. At temperatures above 210°C, the skin layer did not appear even when the flow rate reached 80 g/min. Below 185°C, the torque became excessively high for any screw rotation speed. Accordingly, further experiments were carried out between 185 and 210°C.

Figures 7(a)–(c) show the polarized optical micrographs of the same sample at different magnifications. The experimental conditions were temperature = 200°C, flow rate = 73.9 g/min, and rest time = minimum. Two different layers are clearly discernible from these pictures: Figure 7(c) shows that the thin layer consists of an oriented lamella structure and the core region consists of spherulites.

Figure 8 shows the normalized thickness of the skin layer as a function of the distance from the die entrance at 190°C. The normalized thickness of the skin layer increases with increasing distance from the die entrance. The slope increases with increasing flow rate, but decreases with increasing distance from the die entrance.

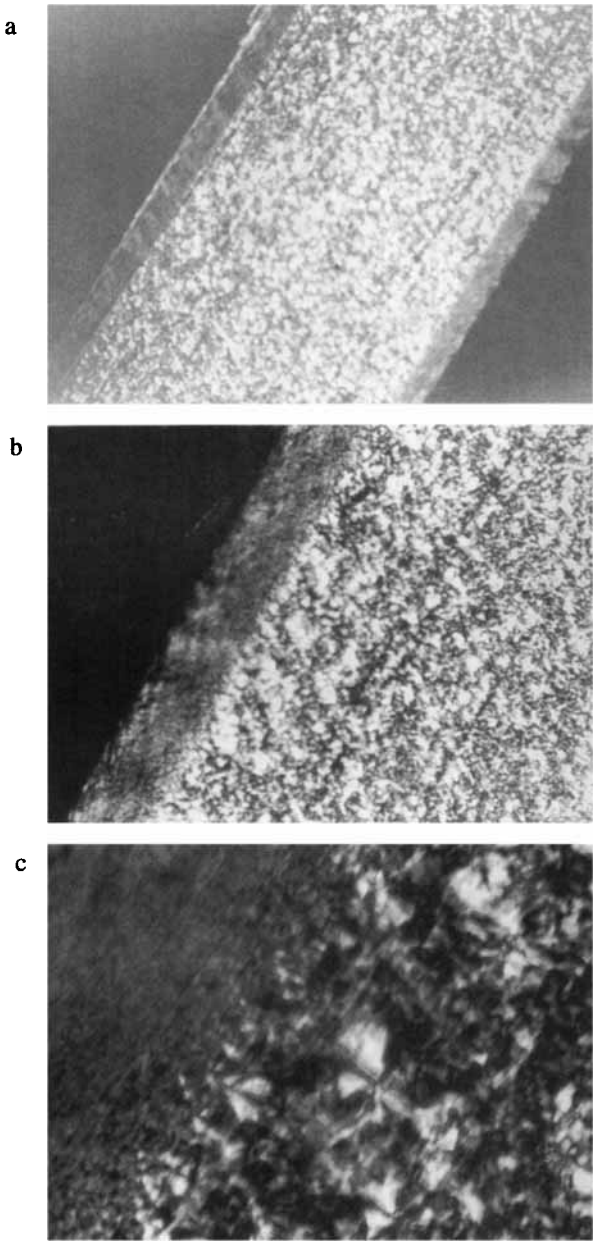

Figure 7 Optical photomicrographs of an extrusion and quenched sample at various magnifications: (a) ×40; (b) ×100; (c) ×400.

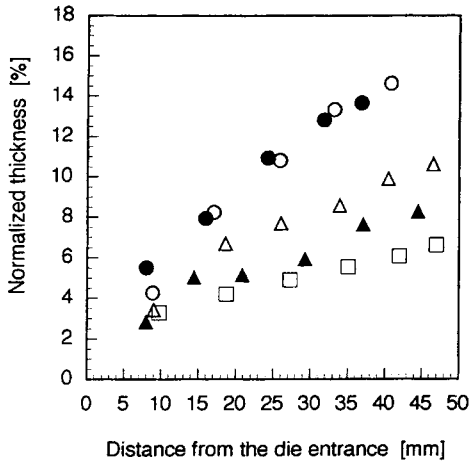

Figure 8 Normalized thickness of shear-induced crystallization layer as a function of distance from die entrance at 190°C: (○) 58.8 g/min; (●) 46.6 g/min; (△) 37.9 g/min; (▲) 33.0 g/min; (□) 32.2 g/min.

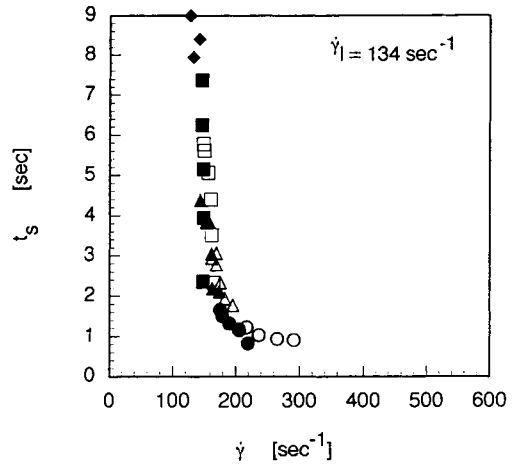

Figure 10 Shearing (residence) time as a function of shear rate at 190°C: (○) 58.8 g/min; (●) 46.6 g/min; (△) 37.9 g/min; (▲) 33.0 g/min; (□) 32.2 g/min; (■) 29.8 g/min; (♦) 28.1 g/min.)

Limiting Shear Rate for Shear-induced Crystallization

Figure 9 is a schematic diagram illustrating the formation of a skin layer during shear flow. As a fluid particle moves downstream along its flow path, its shearing (residence) time t_s in the flow channel increases. Therefore, the thickness of the skin layer increases with increasing distance from the die entrance, even though the shear rate at the interface between the skin layer and the core region decreases as the skin layer thickens. From Figure 9 it is seen that the shearing time t_s' of a fluid particle farther downstream is greater than t_s and the corresponding $\dot{\gamma}'$ is smaller than $\dot{\gamma}$. Since shear rates higher than 100 s^{-1} lie in the power-law region (see Fig. 2), they can be calculated by assuming power-law behavior for the fluid. Figure 10 shows the residence times of all points along the interface vs. the corresponding shear rates at 190°C. It is seen that the data points for various flow rates fall practically on a single curve. With decreasing flow rate, the shear rate

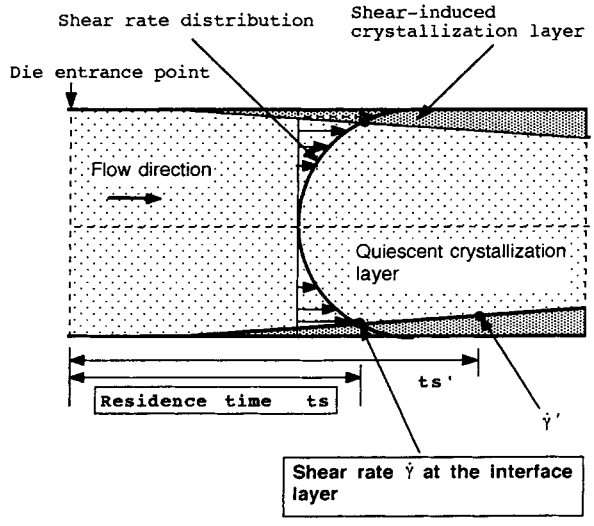

Figure 9 Schematic diagram indicating formation of shear-induced crystallization layer during extrusion.

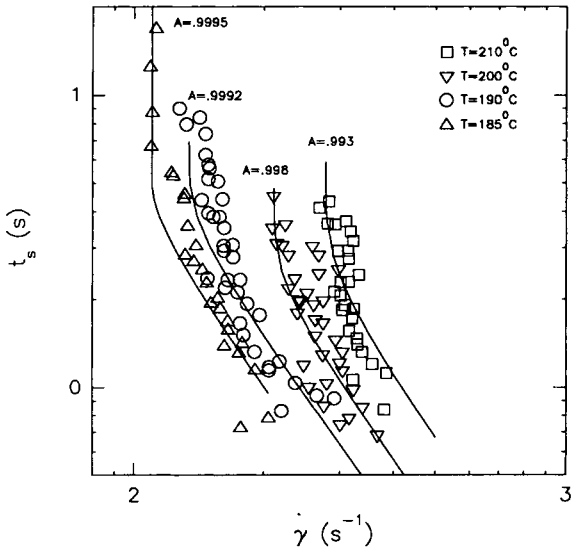

Figure 11 Shearing time vs. shear rate from extrusion experiments at various flow rates and temperatures. Different symbols represent experimental data obtained at temperatures indicated. Solid lines represent fitted values.

Table II Temperature Dependence of Limiting Shear Rate and Parameter A

Temperature (°C)	Limiting Shear Rate (s^{-1})	A
185	109	0.9995
190	134	0.9992
200	211	0.998
210	278	0.993

reaches a limiting value at which the residence time t_s approaches infinity. In other words, it takes an infinite shearing time for the skin layer to form at shear rates below about 130 s^{-1}. The average of the three lowest shear rates shown in the figure is taken as the limiting shear rate $\dot{\gamma}_l$. The double logarithmic plots of shearing time t_s vs. shear rate at different temperatures are combined in Figure 11, from which values of the limiting shear rate $\dot{\gamma}_l$ and parameter A are determined by fitting eq. (12) to the experimental data. The values so obtained are given in Table II. From these values, the critical shear rate of activation $\dot{\gamma}_a$ can be calculated from eq. (13). In Figure 12, ln $\dot{\gamma}_a$ is plotted against $1/T$. The best fit of eq. (6) to the data gives $\dot{\gamma}_{a0} = 4.361 \times 10^{19}$ s^{-1} and $E_a/R = 2.032 \times 10^4$ K. It can be seen from Table II that the value of A approaches unity as the temperature drops below 185°C, with the implication that the growth rate is about the same in quiescent and shear-induced crystallization. This is consistent

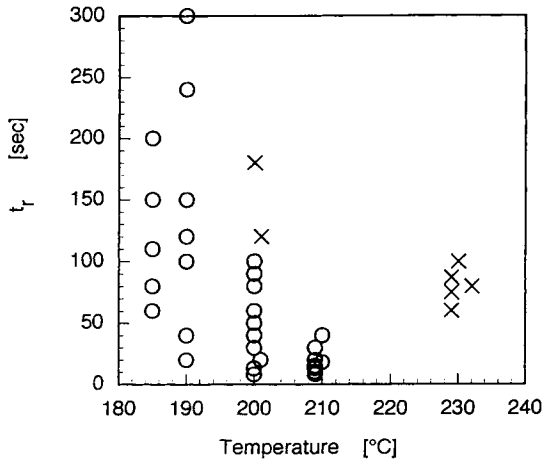

Figure 13 Experimental conditions for existence of shear-induced crystallization layer in experiments with rest times.

with the experimental results of Wolkowicz[25] that the effect of shear on crystallization was mainly to increase the number of nuclei, with no significant change in the growth rate.

Relaxation Behavior of Shear-induced Crystallization Layer

In these experiments, the inner part was kept in the die assembly for various rest times t_r after stoppage of flow and before quenching. Figure 13 shows whether a skin layer exists at various rest times and

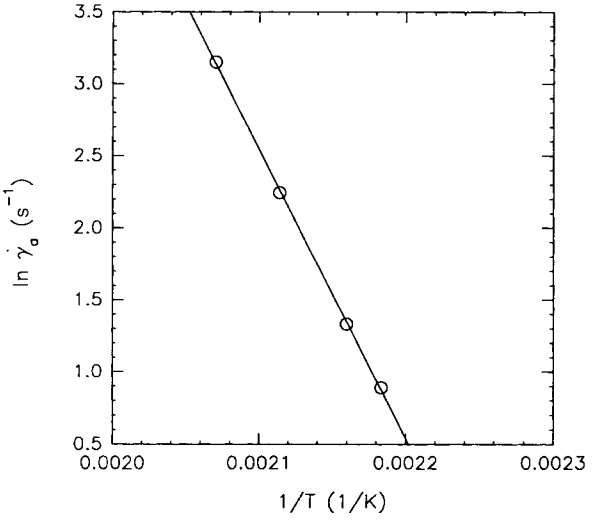

Figure 12 Natural logarithm of critical shear rate of activation as a function of reciprocal temperature. Symbols and lines represent experimental and fitted values, respectively.

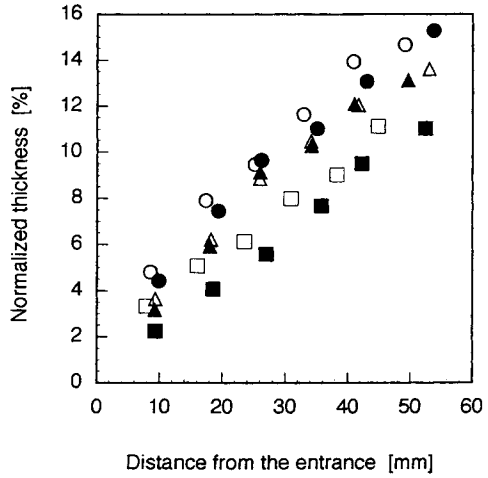

Figure 14 Normalized thickness of shear-induced crystallization layer as a function of distance from die entrance at a flow rate of 72 g/min, a temperature of 200°C, and various rest times: (○) 13 s; (●) 20 s; (△) 40 s; (▲) 50 s; (□) 80 s; (■) 90 s.

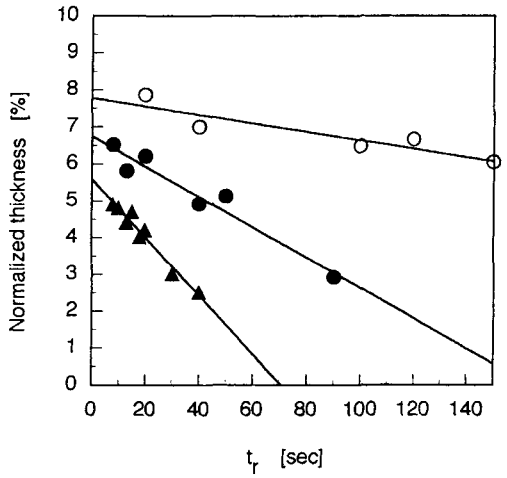

Figure 15 Normalized thickness of shear-induced crystallization layer at 15 mm from die entrance as a function of rest time t_r at a flow rate of 75 g/min: (○) 190°C; (●) 200°C; (▲) 210°C.

temperatures. The symbol "○" stands for the existence of a skin layer, whereas the symbol "×" indicates that no skin layer can be obtained. It is obvious from Figure 13 that the minimum rest time after which a skin layer can no longer exist decreases with increasing temperature. Figure 14 shows plots of the normalized thickness of the skin layer as a function of the distance from the die entrance after several rest times at 200°C. The layer thickness decreases with increasing rest time: a clear indication that relaxation of the skin layer occurred during the rest time.

Figure 15 shows the normalized thickness of the skin layer as a function of rest time at three different temperatures. The thickness of the skin layer decreases linearly with increasing rest time. The negative slope increases in magnitude with increasing temperature, i.e., the rate of relaxation becomes higher as the temperature increases. The shear rate is high and the polymer molecules are highly oriented in the skin layer. Therefore, the birefringence or the difference in refractive index between the directions parallel and perpendicular to the flow direction is larger in the skin layer than in the core region. As a result, birefringence measurements can be used to estimate the growth or relaxation of the skin layer. In Figure 16, the natural logarithm of the birefringence Δn is plotted against the rest time t_r at four different temperatures. It was possible to keep the flow rate relatively constant as the melt temperature varied from 190 to 210°C. The same flow rate could not be maintained at 185°C because of the significantly higher melt viscosity at this temperature. All birefringence measurements were made at a point 15 mm from the die entrance. It was found that the birefringence varied only slightly within the thickness of the skin layer and along the distance from the die entrance. The results are seen well fitted to a linear function of the form

$$\ln \Delta n = \ln \Delta n_0 - \frac{t_r}{\tau} \tag{20}$$

where τ, the relaxation time, can be obtained from the slope. The intercept on the Δn axis, which is the natural logarithm of the initial birefringence, increases with decreasing temperature from 210 to 190°C, whereas the value at 185°C was lower than that at 210°C. This can be explained by the fact that the flow rate at 185°C was only about half of that at the higher temperatures. The initial birefringence between 190 and 210°C was determined by the temperature alone, whereas the value at 185°C was significantly reduced by the lower flow rate attainable. It can also be seen from Figure 16 that the slope increases with increasing temperature from 185 to 210°C. The slope, which is related to the relaxation time, seemed to be insensitive to variations in the flow rate. However, positive conclusions on this point can only be made after further investigations. The values of the relaxation time are given in Table III for the temperatures of 185, 190, 200, and 210°C. The relaxation times are plotted in the form of ln τ vs. $1/T$ in Figure 17. The four data

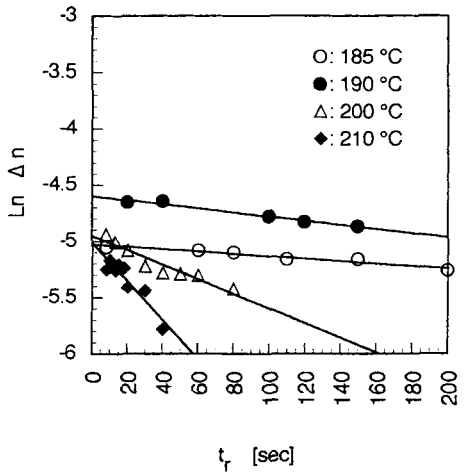

Figure 16 Natural logarithm of birefringence as a function of rest time t_r at various temperatures indicated and a flow rate of 75 g/min, except for 185°C where flow rate was 43 g/min. Various symbols represent experimental values and solid lines represent fitted values.

points are nicely fitted by eq. (7), giving $\tau_0 = 1.735 \times 10^{-21}$ s and $E_\tau/R = 2.5027 \times 10^4$ K. With these parameter values, eq. (7) gives a relaxation time of 3 s at 220°C. Therefore, it should not be surprising now that according to Figure 13 no skin layer could be obtained no matter what the flow rate was. Any shear-induced crystallization would have relaxed within the 10 s or so between the stoppage of flow and the cooling of the central part of the die assembly down to a temperature at which crystallization was possible.

In Figure 16, the data are more scattered at the higher temperatures (200 and 210°C) than at the lower temperatures (185 and 190°C). It was estimated[61] that it took about 8 s for the central part of the die assembly to cool down to the equilibrium melting point of 172°C during quenching from 200 to 20°C. This was in addition to the 2 s or so that had been taken to loosen the retaining bolt and drop the inner part into the cooling water. All in all, this would introduce an error in the measurements of relaxation time especially at high temperatures where the relaxation times are short.

Let us compare the relaxation of shear-induced crystallization with the viscoelastic relaxation of the sheared melt after cessation of flow. For this purpose, it is useful to use a Maxwell element to describe the rheological behavior of the melt. Stress relaxation of the Maxwell element is given by

$$\sigma = \sigma_0 \exp\left(-\frac{t}{\lambda}\right) \tag{21}$$

where σ_0 is the initial stress; t, the time; and $\lambda = \eta_d/G$ is the time taken for the stress to decay to $1/e$ of its initial value. Since the modulus G of the spring is independent of temperature, the relaxation time λ and the viscosity η_d of the dashpot should have the same temperature sensitivity. In Figure 17, the zero shear viscosity η_0 is plotted alongside the relaxation time τ for shear-induced crystallization against the reciprocal temperature. If τ and λ were the same, the two lines in Figure 17 would have the same slope. It is obvious from Figure 17 that this is not the case, i.e., the temperature sensitivity of the relaxation time for shear-induced crystallization is higher than that of the relaxation time of the Maxwell element. The same result was obtained by Janeschitz-Kriegl and co-workers[1,36,62] who suggested that this is indirect evidence of the formation of precursors of shear-induced nucleation in the flow field. These precursors must be very small, for they cannot be detected by flow birefringence[29] and other rheological techniques. The existence of precursors in the form of liquid fibrils has been proposed by McHugh and co-workers.[63,64]

Table III Temperature Dependence of Relaxation Time for Shear-induced Crystallization

Temperature (°C)	Relaxation Time (s)
185	935
190	543
200	155
210	58

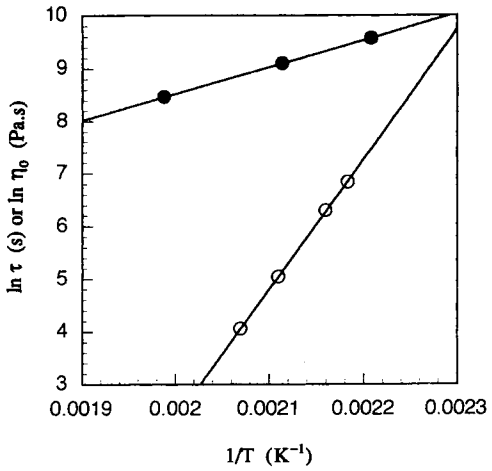

Figure 17 Natural logarithm of relaxation time for shear-induced crystallization and zero-shear viscosity as a function of reciprocal temperature. Hollow and filled circles represent experimental values of relaxation time and zero-shear viscosity, respectively. Solid lines represent fitted values.

CONCLUSIONS

Various characterization experiments were performed on a PP. Viscosity as a function of shear rate and temperature was measured using a rotational rheometer in the cone-and-plate mode at low shear rates and a capillary rheometer at high shear rates. Heat-flow properties, characterizing kinetics and induction time of quiescent crystallization, were obtained from nonisothermal DSC measurements. Material data characterizing shear-induced crystallization were obtained from a special kind of extrusion experiments through a slit die with subsequent quenching of the material in the die after various rest times. A thin skin layer consisting of an oriented

lamella structure was observed under an optical microscope. The skin layer thickness was found to increase with increasing distance from the die entrance. The limiting shear rate below which no skin layer could be obtained increased with increasing temperature. The skin layer thickness decreased with increasing rest time between the cessation of flow and the quenching of the sample in the die, indicating that a relaxation process was taking place. The relaxation time for shear-induced crystallization was determined by measuring the birefringence of the skin layer in samples obtained at different rest times. It was found that the relaxation time for shear-induced crystallization was significantly different from the characteristic time for viscoelastic relaxation of the sheared melt after the cessation of flow. A model developed by Janeschitz-Kriegl and co-workers was used to describe the shear-induced crystallization kinetics. All three parameters in the model were found to be strongly dependent on temperature. The model parameters could only be obtained within a narrow range of temperatures using the present extrusion experiments. It was found that both $\dot{\gamma}_a(T)$ and $\tau(T)$ could be well represented by an Arrhenius-type temperature dependence between 185 and 210°C.

Financial support from the Ohio Board of Regents is gratefully acknowledged. The polypropylene used in this work was kindly supplied by Himont USA, Inc.

REFERENCES

1. G. Eder, H. Janeschitz-Kriegl, and S. Liedauer, *Prog. Polym. Sci.*, **15,** 629 (1990).
2. M. R. Kantz, D. Newman, and F. H. Stigale, *J. Appl. Polym. Sci.*, **16,** 1249 (1972).
3. D. R. Fitchmun and Z. Mencik, *J. Polym. Sci. Polym. Phys. Ed.*, **11,** 951 (1973).
4. Z. Mencik and D. R. Fitchmun, *J. Polym. Sci. Polym. Phys. Ed.*, **11,** 973 (1973).
5. M. R. Kantz, *Int. J. Polym. Mater.*, **3,** 245 (1974).
6. M. Fujiyama, *Kobunshi Ronbunshu*, **32,** 411 (1975).
7. S. Y. Hobbs and C. F. Pratt, *J. Appl. Polym. Sci.*, **19,** 1701 (1975).
8. G. Menges, G. Wubken, and B. Horn, *Colloid Polym. Sci.*, **254,** 267 (1976).
9. M. Fujiyama and K. Azuma, *J. Appl. Polym. Sci.*, **23,** 2807 (1979).
10. M. R. Kamal and F. H. Hoy, *J. Appl. Polym. Sci.*, **28,** 1787 (1983).
11. J. P. Trotignon and J. Verdu, *J. Appl. Polym. Sci.*, **34,** 1 (1987).
12. M. Fujiyama, T. Wakino, and Y. Kawasaki, *J. Appl. Polym. Sci.*, **35,** 29 (1988).
13. E. Fleischmann, P. Zipper, A. Janosi, W. Geymayer, J. Koppelmann, and J. Schurz, *Polym. Eng. Sci.*, **29,** 835 (1989).
14. C. S. Hindle and J. R. White, *Polym. Eng. Sci.*, **32**(3), 157 (1992).
15. H. Ayrom and M. Cakmak, in *Proceedings of the 10th PPS Annual Meeting,* Akron, 1994, p. 103.
16. S. S. Katti and M. Schultz, *Polym. Eng. Sci.*, **22,** 1001 (1982).
17. K. Kobayashi and T. Nagasawa, *J. Macromol. Sci.-Phys. B*, **4,** 331 (1970).
18. T. W. Haas and B. Maxwell, *Polym. Eng. Sci.*, **9,** 225 (1969).
19. A. Wereta and C. G. Gogos, *Polym. Eng. Sci.*, **11,** 19 (1971).
20. T. Amano, S. Kajita, and K. Katayama, *Prog. Colloid Polym. Sci.*, **58,** 108 (1975).
21. R. R. Lagasse and B. Maxwell, *Polym. Eng. Sci.*, **16,** 189 (1976).
22. K. Katayama, S. Murakami, and K. Kobayashi, *Bull. Inst. Chem. Res. Kyoto Univ.*, **54,** 81 (1976).
23. R. D. Ulrich and F. P. Price, *J. Appl. Polym. Sci.*, **20,** 1077 (1976).
24. C. H. Sherwood, F. P. Price, and R. S. Stein, *J. Polym. Sci. Polym. Symp.*, **63,** 77 (1978).
25. M. D. Wolkowicz, *J. Polym. Sci. Polym. Symp.*, **63,** 365 (1978).
26. H. Janeschitz-Kriegl, G. Eder, G. Krobath, and S. Liedauer, *J. Non-Newtonian Fluid Mech.*, **23,** 107 (1987).
27. H. Janeschitz-Kriegl, R. Wimberger-Friedl, G. Krobath, and S. Liedauer, *Kautschuk+Gummi Kunststoffe,* **40,** 301 (1987).
28. M. C. Chien and R. A. Weiss, *Polym. Eng. Sci.*, **28,** 6 (1988).
29. G. Eder, H. Janeschitz-Kriegl, and G. Krobath, *Prog. Colloid Polym. Sci.*, **80,** 1 (1989).
30. B. Monasse and C. Fryda, in *Proceedings of the 6th PPS Annual Meeting,* Nice, 1990, P06-02.
31. S. P. Kim and S. C. Kim, *Polym. Eng. Sci.*, **33,** 83 (1993).
32. S. Liedauer, G. Eder, H. Janeschitz-Kriegl, P. Jerschow, W. Geymayer, and E. Ingolic, *Int. Polym. Process.*, **8,** 236 (1993).
33. J. Moitzi and P. Skalicky, *Polymer*, **34,** 3168 (1993).
34. G. Titomanlio and V. Brucato, in *Proceedings of the 10th PPS Annual Meeting,* Akron, 1994, p. 93.
35. G. Eder and H. Janeschitz-Kriegl, *Colloid Polym. Sci.*, **266,** 1087 (1988).
36. H. Janeschitz-Kriegl and G. Eder, *J. Macromol. Sci.-Chem. A*, **27,** 1733 (1990).
37. M. R. Kamal and P. G. Lafleur, *Polym. Eng. Sci.*, **24,** 692 (1984).
38. V. M. Nadkarni and J. P. Jog, *Plast. Eng.*, **August,** 37 (1984).
39. P. G. Lafleur and M. R. Kamal, *Polym. Eng. Sci.*, **26,** 92 (1986).
40. M. R. Kamal and P. G. Lafleur, *Polym. Eng. Sci.*, **26,** 103 (1986).

41. L. T. Manzione, *SPE Tech. Pap.*, **33,** 285 (1987).
42. N. J. McCaffrey, C. Friedl, and R. Thomas, *SPE Tech. Pap.*, **36,** 382 (1990).
43. W. Y. Chiu, H. J. Tai, L. W. Chen, and L. H. Chu, *J. Appl. Polym. Sci.*, **43,** 521 (1991).
44. T.-Y. Chen, V. W. Wang, and M. J. Bozarth, *SPE Tech. Pp.*, **38,** 72 (1992).
45. C. M. Hsiung and M. Cakmak, *Polym. Eng. Sci.*, **31,** 1372 (1991).
46. J. M. Haudin and N. Billon, *Prog. Colloid Polym. Sci.*, **87,** 132 (1992).
47. A. I. Isayev, T. W. Chan, M. Gmerek, and K. Shimojo, *J. Appl. Polym. Sci.*, **55,** 821 (1995).
48. M. M. Cross, *Rheol. Acta*, **18,** 909 (1979).
49. K. Nakamura, K. Katayama, and T. Amano, *J. Appl. Polym. Sci.*, **17,** 1031 (1973).
50. R. M. Patel and J. E. Spruiell, *Polym. Eng. Sci.*, **31,** 730 (1991).
51. J. D. Hoffman, G. T. Davis, and J. I. Lauritzen, in *Treatise on Solid State Chemistry: Crystalline and Non-Crystalline Solids*, J. B. Hannay, Ed., Plenum, New York, 1976, Vol. 3.
52. W. L. Sifleet, N. Dinos, and J. R. Collier, *Polym. Eng. Sci.*, **13,** 10 (1973).
53. Yu.K. Godovsky and G. L. Slonimsky, *J. Polym. Sci. Polym. Phys. Ed.*, **12,** 1053 (1974).
54. G. Eder, H. Janeschitz-Kriegl, and S. Liedauer, *Prog. Colloid Polym. Sci.*, **87,** 129 (1992).
55. W. Schneider, A. Koppl, and J. Berger, *Int. Polym. Proc.*, **2,** 151 (1988).
56. W. Schneider, J. Berger, and A. Koppl, in *Proceedings of the 1st International Conference on Transport Phenomena in Processing*, S. I. Guceri, Ed., Technomic, Lancaster-Basel, 1993, p. 1043.
57. H. Janeschitz-Kriegl, H. Wippel, Ch. Paulik, and G. Eder, *Colloid Polym. Sci.*, **271,** 1107 (1993).
58. T. W. Chan and A. I. Isayev, *Polym. Eng. Sci.*, **34,** 461 (1994).
59. T. W. Chan, K. Shimojo, and A. I. Isayev, *SPE Tech. Pap.*, **39,** 1032 (1993).
60. D. W. van Krevelen, *Properties of Polymers*, Elsevier, Amsterdam, 1976.
61. K. Shimojo, Master's Thesis, University of Akron, Akron, Ohio, 1993.
62. H. Janeschitz-Kriegl, *Prog. Colloid Polym. Sci.*, **87,** 117 (1992).
63. J. Rietveld and A. J. McHugh, *J. Polym. Sci. Polym. Lett. Ed.*, **21,** 919 (1983).
64. A. J. McHugh and J. A. Spevacek, *J. Polym. Sci. Polym. Phys. Ed.*, **29,** 969 (1991).

Received May 16, 1994
Accepted July 19, 1994